Structural Damage Diagnosis Using Interstory Drift–Based Acceleration Feedback with Test Validation

Jiazeng Shan[1]; Henry T. Y. Yang, M.ASCE[2]; Weixing Shi[3]; Daniel Bridges[4]; and Paul K. Hansma[5]

Abstract: This study presents a numerical structural damage detection method using interstory drift–based structural acceleration measurements in the time domain. The coupling effect of the damage at different locations in the multiple-degree-of-freedom building system is eliminated by projecting the measured accelerations onto specific independent subspaces. The damage in a region will only affect the output of the designed monitor observing the substructure within the region. The severity of the damage is estimated numerically using a model-based prediction curve of stiffness change. Results obtained by the present numerical simulations for the illustrative examples are validated by experimental investigations using a 3-story aluminum frame structure and a 12-story concrete frame structure, and the numerical simulation results are compared with some representative experimental data with favorable correlations. Incorporation of the incomplete measurement, different structural materials, and different excitations into the method are studied and discussed. **DOI: 10.1061/(ASCE)EM.1943-7889.0000531.** © *2013 American Society of Civil Engineers.*

CE Database subject headings: Damage; Structural dynamics; Frames; Excitation; Drift; Tests; Validation.

Author keywords: Damage assessment; Structural dynamics; Frame structures; Excitations.

Introduction

Health monitoring of a civil infrastructure before, during, and after disastrous events constitutes an important task for structural engineers to maintain the structural integrity. Generally, structural health monitoring is involved with evaluating the state of health of the structures, determining the severity and locations of the damage, assessing the deterioration within the structure, and even the feasibility of repair. Such monitoring processes can provide necessary information for structural control, maintenance, retrofit, and other relevant activities to ensure the structural integrity and safety.

Currently, many state-of-the-art health monitoring methods are referred to as global health monitoring methods and can be categorized into three main groups. One group makes use of the shifts or changes in structural model parameters such as resonant frequencies, modal damping, or mode shapes as the damage indicator to assess the structural health condition (Pandey et al. 1991; Salawu 1997; Curadelli et al. 2008). Another group of existing techniques, termed as the matrix update method, uses the structural modal matrices including stiffness, flexibility, and damping matrices to match measured data (Liu 1995; Gao et al. 2007). These two approaches usually are known as the model-based structural health monitoring (SHM) methods. An extensive survey of the global vibration-based methods can be found in Doebling et al. (1996). The third approach of health monitoring is related to the linear or nonlinear system identification in the time domain, such as the least square method (Yang et al. 2007), the ensemble Kalman filter (Ghanem and Ferro 2006), the extended Kalman filter (Yang et al. 2006), and the Bayesian probabilistic technique (Vanik et al. 2000).

Interstory drift, defined as the relative translational displacement between two consecutive floors, is well known as an important engineering response parameter and indicator of structural performance and damage. Skolnik and Wallace (2010) discussed several issues associated with double integration of measured acceleration and presented alternative methods for obtaining interstory drift. The extended parameter, interstory drift ratio, is one of the key response quantities in earthquake structural engineering and is associated to the structural health condition and performance (Celebi et al. 2004; Porter et al. 2006).

In previous studies by Ma et al. (2005) and Sebastijanovic et al. (2010), a series of feedback methods for structural damage identification in the time domain have been developed through decomposition of the coupling effect of the structural damage. The measured structural responses were assumed to be displacements, velocities, and accelerations. Comparisons with accelerations, displacements, and velocities are not as readily and accurately measurable in practice. However, in the previous acceleration feedback method, the measured acceleration response became the velocity of the new assumed system. An obvious difficulty encountered was the calculation of the time derivative of the ground acceleration input (Sebastijanovic et al. 2010). The basic linear central finite-difference technique was used in this previous research, with a sensitive requirement on the choice of time interval Δt. It is generally recognized that there could be numerical deterioration in the time derivatives of the ground accelerations, especially on the high-frequency components, which influences the performance of the designed monitors.

[1]Ph.D. Candidate, Research Institute of Structural Engineering and Disaster Reduction, Tongji Univ., Shanghai 200092, China.

[2]Professor, Dept. of Mechanical Engineering, Univ. of California, Santa Barbara, CA 93106 (corresponding author). E-mail: henry.yang@chancellor.ucsb.edu

[3]Professor, Research Institute of Structural Engineering and Disaster Reduction, Tongji Univ., Shanghai 200092, China.

[4]Research Associate, Dept. of Physics, Univ. of California, Santa Barbara, CA 93106.

[5]Professor, Dept. of Physics, Univ. of California, Santa Barbara, CA 93106.

Note. This manuscript was submitted on February 23, 2012; approved on August 12, 2012; published online on August 23, 2012. Discussion period open until February 1, 2014; separate discussions must be submitted for individual papers. This paper is part of the ***Journal of Engineering Mechanics***, Vol. 139, No. 9, September 1, 2013. ©ASCE, ISSN 0733-9399/2013/9-1185–1196/$25.00.

In this paper, a damage detection algorithm using acceleration measurements is proposed. The formulations of the method are first discussed. A 3-story lumped-mass model used in the previous study is considered in the present numerical simulation, and the damage tracking performance is compared with that of the previous methods. Then two illustrative structures, a 3-story aluminum structure with simulated stiffness changes and a 12-story concrete structure with developed damages, are built to experimentally investigate the present damage detection algorithm with shaking table tests. It was found that the currently proposed time-domain method exhibits favorable performance in the numerical simulation and also provides favorable correlations with some representative data obtained from the tests of the two illustrative examples.

Formulation

A structural system such as a multistory building can commonly be modeled in extreme simplicity as a lumped-mass or shear-beam structure. The governing equation of such a linear model under external excitations can be written as

$$M\ddot{z} + C\dot{z} + (K + \Delta K)z = Du \tag{1}$$

where z = displacement vector; $\dot{z}$ and $\ddot{z}$ = velocity and acceleration vectors, respectively; u = excitation vector, and in the case of seismic excitation, it is a scalar representing the ground acceleration; and matrices M, C, and K = mass, damping, and stiffness matrices of the undamaged structure, respectively. Matrix D determines the location of the excitation. Matrix ΔK contains the information of the damage present in the structure. For a healthy structure, ΔK contains zeros. Eq. (1) consists of a series of linear differential equations, which can be written generally as Eqs. (2) and (3) for seismic excitations from the force equilibrium consideration

$$\sum_{i=1}^{n} m_i\ddot{z}_i + c_1\dot{z}_1 + (k_1 + \Delta k_1)z_1 = -\sum_{i=1}^{n} m_i u \tag{2}$$

$$\sum_{i=j}^{n} m_i\ddot{z}_i + c_j\left(\dot{z}_j - \dot{z}_{j-1}\right) + \left(k_j + \Delta k_j\right)\left(z_j - z_{j-1}\right) = -\sum_{i=j}^{n} m_i u, \quad n \geq j \geq 2 \tag{3}$$

where n = total number of degrees of freedom of the system, and j = floor number of the corresponding matrices or vectors.

For generality and simplicity, the following formulations are based on Eq. (3), which can be written as

$$m_j\ddot{z}_j + c_j\left(\dot{z}_j - \dot{z}_{j-1}\right) + \left(k_j + \Delta k_j\right)\left(z_j - z_{j-1}\right) = -\sum_{i=j}^{n} m_i u - \sum_{i=j+1}^{n} m_i\ddot{z}_i \tag{4}$$

Eq. (4) can then be written as

$$m_j\left(\ddot{z}_j - \ddot{z}_{j-1}\right) + c_j\left(\dot{z}_j - \dot{z}_{j-1}\right) + k_j\left(z_j - z_{j-1}\right) = -\sum_{i=j}^{n} m_i u - \sum_{i=j+1}^{n} m_i\ddot{z}_i - \Delta k_j\left(z_j - z_{j-1}\right) - m_j\ddot{z}_{j-1} \tag{5}$$

Defining a new variable (interstory drift of the jth story) as

$$Y_j = z_j - z_{j-1} \tag{6}$$

Then, Eq. (5) becomes

$$m_j\ddot{Y}_j + c_j\dot{Y}_j + k_jY_j = -\sum_{i=j}^{n} m_i u - \sum_{i=j+1}^{n} m_i\ddot{z}_i - \Delta k_j\left(z_j - z_{j-1}\right) - m_j\ddot{z}_{j-1} \tag{7}$$

If a nominal external force is defined as

$$p_j = -\sum_{i=j}^{n} m_i u - \sum_{i=j+1}^{n} m_i\ddot{z}_i - m_j\ddot{z}_{j-1} \tag{8}$$

Eq. (7) can then be written as

$$m_j\ddot{Y}_j + c_j\dot{Y}_j + k_jY_j = p_j - \Delta k_j\left(z_j - z_{j-1}\right) \tag{9}$$

When $j = 1$ and $Y_1 = z_1$, Eq. (9) becomes

$$m_1\ddot{Y}_1 + c_1\dot{Y}_1 + k_1Y_1 = p_1 - \Delta k_1 z_1$$

$$p_1 = -\sum_{i=1}^{n} m_i u - \sum_{i=2}^{n} m_i\ddot{z}_i \tag{10}$$

The variable Y_j = interstory drift of the corresponding story and has the same unit as z_j. The system described in Eq. (9) is equivalent to a lumped-mass model with one degree of freedom. Because no special or additional assumptions were made in deriving Eq. (9), all systems that can be described by Eqs. (2) and (3) can be reduced to single-degree-of-freedom (SDOF) systems. Another characteristic observed from Eq. (9) is that among all the possible locations of damage $[\Delta k_1, \ldots, \Delta k_j, \ldots, \Delta k_n]$, only Δk_j affects this SDOF system in Eq. (9), whereas the effects of damage on other stories are eliminated. Compared with Eqs. (4) and (5) in Ma et al. (2005), it is noted that the arbitrarily chosen virtual damping ratio ζ and natural frequency ω no longer exist in this new algorithm, whereas the weighted output variable is now a structural response parameter.

Eqs. (9) and (10) correspond to the current state of the structure, which could be either damaged ($\Delta k_j \neq 0$) or undamaged ($\Delta k_j = 0$). For damage assessment, it is necessary to construct a virtual healthy system subjected to the same input excitation as a reference for comparison. The dynamic equation for this virtual healthy system can be expressed directly as

$$m_j\ddot{Y}_j^r + c_j\dot{Y}_j^r + k_jY_j^r = p_j; \quad j = 1 \sim n \tag{11}$$

where Y_j^r = interstory drift of the jth story of the virtual healthy system. Conceptually from the previous discussion, structural damage represented by reduction in stiffness can be identified when the actual interstory responses $[\ddot{Y}_j, \dot{Y}_j, Y_j]$ deviates from the estimated virtual responses $[\ddot{Y}_j^r, \dot{Y}_j^r, Y_j^r]$. Subtracting Eq. (9) from Eq. (11), the following response-damage relationship can be established:

$$m_j\ddot{r}_j + c_j\dot{r}_j + k_jr_j = \Delta k_j\left(z_j - z_{j-1}\right)$$

$$\ddot{r}_j = \ddot{Y}_j^r - \ddot{Y}_j; \quad j = 2 \sim n \tag{12}$$

especially when $j = 1$

$$m_1\ddot{r}_1 + c_1\dot{r}_1 + k_1r_1 = \Delta k_1 z_1$$

$$\ddot{r}_1 = \ddot{Y}_1^r - \ddot{Y}_1 \tag{13}$$

J. Eng. Mech. 2013.139:1185-1196.

Apparently, the algorithms thus derived are applicable to all kinds of structural dynamic response measurements such as displacements, velocities, and accelerations. For the sake of practicability in engineering application, the quantity $\ddot{r}_j$ is chosen to be the weighted monitor output, which will generally be nonzero for a damage occurrence on the jth story when $\Delta k_j \neq 0$. The presence of the corresponding story damage can be directly determined by examining the value of $\ddot{r}_j$ that is the output of the designed monitor.

The state-space oriented description is adopted herein to study the linear system other than its counterpart described by higher-order differential equations. The state vector is defined as $x_i = [Y_i, \dot{Y}_i]^T$ for the ith story and the measurement vector $w = [\ddot{z}_1, \ddot{z}_2, \ldots, \ddot{z}_n]^T$. To be consistent with the traditional structural dynamic equations, here the measurements $\ddot{z}$ are the story accelerations relative to the ground that can be straight forwardly obtained from the measured absolute accelerations. Thus, acceleration measurement w for the monitors was fixed to be relative accelerations on each floor throughout this paper unless otherwise noted. The equivalent state space representations of health monitor for the actual structure corresponding to Eqs. (11) and (12) can be obtained as follows:

$$\begin{aligned} \dot{x}_i &= A_i x_i + G_i u + E_i w \\ \ddot{r}_i &= \ddot{Y}_i^r - \ddot{Y}_i = C_{r,i} x_i + G_{r,i} u + E_{r,i} w \end{aligned} \tag{14}$$

where

$$A_i = \begin{bmatrix} 0 & 1 \\ -k_i/m_i & -c_i/m_i \end{bmatrix}_{2\times 2}$$

$$G_i = \begin{bmatrix} 0 & -\sum_{j=i}^{n} m_j/m_i \end{bmatrix}^T_{2\times 1}$$

$$E_i = \begin{bmatrix} 0\ldots 0 & 0 & 0 & 0\ldots & 0 \\ 0\ldots 0 & -1 & 0 & -m_{i+1}/m_i \ldots & -m_n/m_i \end{bmatrix}_{2\times n} \tag{15}$$

$$C_{r,i} = [-k_i/m_i \quad -c_i/m_i]_{1\times 2}$$

$$G_{r,i} = -\sum_{j=i}^{n} m_j/m_i$$

$$E_{r,i} = [0\ldots 0 \quad 0 \quad -1 \quad -m_{i+1}/m_i \ldots -m_n/m_i]_{1\times n} \tag{16}$$

for the first story ($i = 1$)

$$E_1 = \begin{bmatrix} 0 & 0 & \ldots & 0 \\ 0 & -m_2/m_1 & \ldots & -m_n/m_1 \end{bmatrix}_{2\times n}$$

$$E_{r,1} = [-1 \quad -m_2/m_1 \ldots -m_n/m_1]_{1\times n} \tag{17}$$

The monitor defined by Eq. (14) is used to assess the health condition of every story in the system. The quantity $\ddot{r}_i$ is the output of the ith monitor and also indicates the discrepancy between the measurement and the estimation. The monitor takes the measurements of the structural response w and the external excitation u as inputs. Because of the behavior of $\ddot{r}_i$ under the influence of structural damages according to Eq. (12), the output of the designed monitor $\ddot{r}_i$ can thus be used as a damage indicator.

Monitor outputs are normalized with respect to the measurements as follows (Ma et al. 2005):

$$\ddot{r}_{norm,i}(t) = \sqrt{\frac{\int_{t-t_h}^{t} \ddot{r}_i^2(\tau)d\tau}{\int_{t-t_h}^{t} \overline{y}_i^2(\tau)d\tau}} \tag{18}$$

where $\ddot{r}_{\mathrm{norm,i}}$ = normalized output for the ith monitor; $\ddot{r}_i$ = output for the ith monitor; y = measurement vector; and t_h = integration time horizon of past measurements used for normalization, noting that $\overline{y}_i(t)$ equals $\ddot{Y}_i = \ddot{z}_i - \ddot{z}_{i-1}$ ($i = 2 \sim n$) and $\overline{y}_1(t) = \ddot{Y}_1 = \ddot{z}_1$. Such normalized output is dimensionless and thus serves as a better indicator for stiffness changes. The selection of t_h has been numerically studied and discussed in detail (Ma et al. 2005; Sebastijanovic et al. 2010).

Numerical Simulation

The illustrative example considered herein was a 3-story shear beam model corresponding to a 3-story frame structure considered previously by Yang et al. (1995). The mass, stiffness, and damping parameters of each floor were assumed to be 1,000 kg, 980 kN/m, and 1.407 kN-s/m, respectively. The damage of every floor was defined as changes in the equivalent stiffness coefficients. The severity of the damage was indicated quantitatively by the percent stiffness change α_i, where i denotes story number. For the original undamaged model $\alpha_i = 0$. The north-south (N-S) component of the ground acceleration of the 1940 El Centro earthquake was used as excitation sources to the present models for the damage studies. The measured structural responses were the absolute accelerations of all the floors. The measurement noise was assumed to have a signal-to-noise ratio (SNR) of 30 dB.

Fig. 1 shows the simulation results of different damage detection scenarios using the presently proposed interstory drift–based acceleration feedback method. For the undamaged model (Case 1), the values of α_1, α_2, and α_3 were all 0. The values of α_1, α_2, and α_3 were chosen as 0, 5, and 10%, respectively, in Case 2 as a damaged model. For Case 3, there was a sudden stiffness changes during the excitation in α_3 from 10 to 25% at the fifth second, whereas $\alpha_1 = 0$ and $\alpha_2 = 25\%$ for the whole time history. The integration time horizon t_h defined in Eq. (18) was chosen to be 4.0 s as a tradeoff as recommended in Ma et al. (2005) to ensure functional quality of the monitor online damage tracking performance and to generate smaller fluctuations of the normalized outputs.

The original and normalized monitor outputs for the first floor, as illustrated in Figs. 1(c and f), are stable and not distinguishable between different cases, indicating similar stiffness conditions. Fig. 1(e) shows that even a 5% stiffness change on the second floor can be noticeably detected with the SNR being 30 dB. Fig. 1(d) shows that before the predetermined damage occurrence time ($t = 5$ s) in Case 3, the normalized monitor outputs of third floor were stable, similar to that as shown in Case 2, indicating similar stiffness conditions between Cases 2 and 3. Shortly after the damage occurrence as assumed at around the fifth second, the monitor output of the third floor in Fig. 1(a) experienced sudden jumps and fluctuations, indicating the occurrence of the assumed damage, which is more apparent in Fig. 1(d) with a sudden rise of the normalized monitor output. Moreover, the normalized monitor output of the third floor became relatively stable and flat after 7 s. Thus, in this example, the online tracking response time was estimated as ~2 s based on the choice of the integration time horizon $t_h = 4$ s.

There are two previously proposed algorithms. One was based on displacement feedback (Ma et al. 2005) and the other was based on acceleration feedback (Sebastijanovic et al. 2010). The normalized

J. Eng. Mech. 2013.139:1185-1196.

monitor outputs from these two methods with the same numerical model and the same stiffness changes as described in Fig. 1 are shown in Fig. 2 for comparison with the interstory drift–based acceleration feedback. All the parameters were kept the same as assumed in the two corresponding publications. The integration time horizon t_h was thus set the same as 4 s. The parameter ζ in the displacement feedback method was equal to 1, whereas ω was 4.74 rad/s. For the previous acceleration feedback method, γ was assumed as 1.

Both of the normalized monitor outputs successfully reveal the stiffness changes in Cases 2 and 3. An observable remark is that the sudden stiffness change described by Case 3 seems to not be apparent in Fig. 2(a), whereas the other two methods were able to clearly illustrate the sudden transition of normalized monitor output pronouncedly in Figs. 1(d) and 2(d), indicating the sudden stiffness change. In both cases, the currently proposed method seems to have demonstrated improved clarity of results than the displacement feedback method and similar performance with the acceleration feedback method in damage tracking performance for the illustrative examples.

Experimental Investigation

The present interstory drift–based acceleration feedback method was evaluated by examples of two experimental structures subjected to dynamic excitations. The first structure constructed was a scaled one-bay 3-story aluminum frame structure as shown in Fig. 3(a), whereas the second structure constructed was a scaled 12-story concrete frame structure as shown in Fig. 3(b).

Three-Story Aluminum Structure and Results

The 3-story aluminum structure was constructed as a shear-beam model as shown in Fig. 3(a) with four aluminum solid rods with a diameter of 0.009 m and a height of 1.68 m to represent columns, plus three aluminum rectangular plates to represent two floors and the roof, each with dimensions of 0.61, 0.51, and 0.013 m for length, width, and thickness, respectively. The mass of each floor of the model was 11.09 kg. In this experiment, the damage was assumed as the interstory stiffness changes on the first floor simulated using

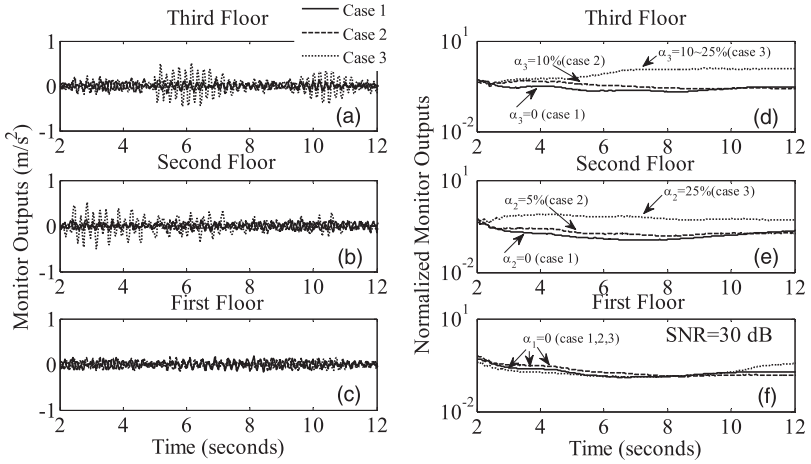

Fig. 1. Damage identification for different scenarios of the 3-story numerical model: (a)–(c) are original monitor outputs for Cases 1–3; (d)–(f) are normalized monitor outputs for Cases 1–3, where in Case 1: $\alpha_1 = \alpha_2 = \alpha_3 = 0$; Case 2: $\alpha_1 = 0$, $\alpha_2 = 5\%$, $\alpha_3 = 10\%$; Case 3: $\alpha_1 = 0$, $\alpha_2 = 25\%$, $\alpha_3 = 10\%$ at $t < 5$ s, $\alpha_3 = 25\%$ at $t \geq 5$ s

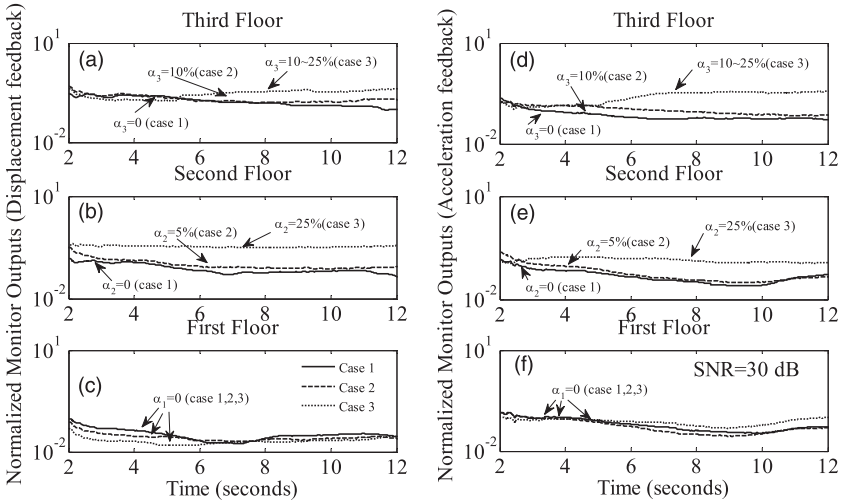

Fig. 2. Damage identification for different scenarios of the 3-story numerical model: (a)–(c) are normalized monitor outputs using the displacement feedback for Cases 1–3; (d)–(f) are normalized monitor outputs using the acceleration feedback for Cases 1–3, where in Case 1: $\alpha_1 = \alpha_2 = \alpha_3 = 0$; Case 2: $\alpha_1 = 0$, $\alpha_2 = 5\%$, $\alpha_3 = 10\%$; Case 3: $\alpha_1 = 0$, $\alpha_2 = 25\%$, $\alpha_3 = 10\%$ at $t < 5$ s, $\alpha_3 = 25\%$ at $t \geq 5$ s

J. Eng. Mech. 2013.139:1185-1196.

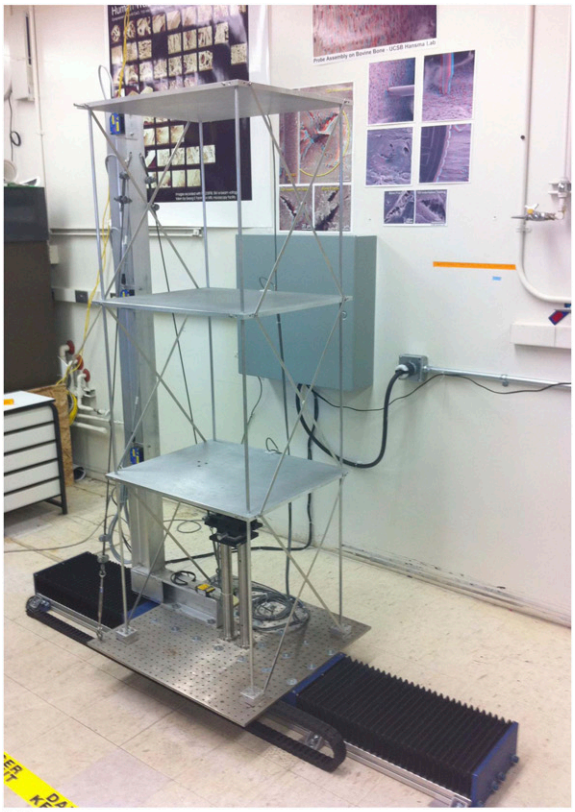

(a)

(b)

Fig. 3. Two experimental structures: (a) 3-story aluminum frame structure; (b) 12-story concrete frame structure

spring attachments with various spring constants. The numerical model is shown in Fig. 4(a) with the spring constants and masses for each floor. The healthy structure was considered as the state with the attached spring in maximum stiffness. In this example, $k_{s,\max} = 2,088.8\,\mathrm{N/m}$. Fig. 4(b) shows the spring device installed to provide the assumed supplemental stiffness of the first floor to generate data for comparison with the present numerical analysis. The spring device needs to be in pairs to provide symmetric stiffness increase in the two opposite directions.

The experimental structure was subjected to excitations simulated by the unidirectional shaking table. The excitation to the structure was assumed as the N-S component of the 1995 Kobe earthquake, and the time interval of the excitation was 0.004 s. The peak acceleration of excitations was $0.2g$. Three sets of stiffness scenarios were conducted with parameters summarized in Table 1. The horizontal displacement and acceleration responses in loading direction were measured on ground and three upper floors.

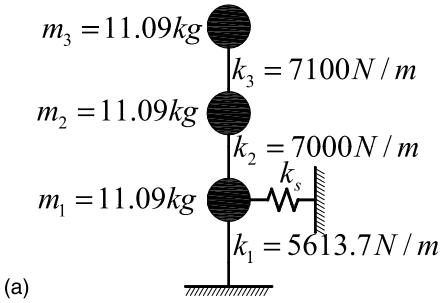

(a)

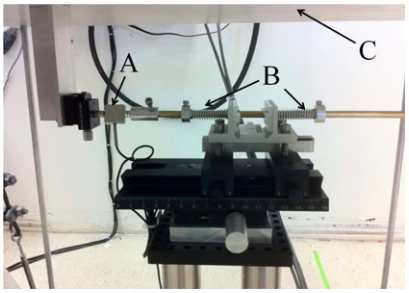

(b)

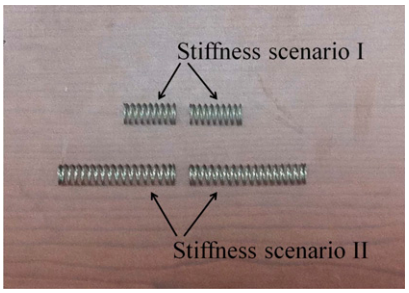

(c)

Fig. 4. (a) Simplified lumped-mass model with attached stiffness k_s; (b) stiffness change device installed to increase stiffness as a means of providing the desired floor stiffness—A, force transducer; B, attached springs; C, first floor plane; (c) two different types of spring pairs for use

Table 1. Summary of the Experimental Setup

Stiffness scenario	Attached stiffness, k_s (N/m)	Time length (s)	Sampling frequency (Hz)	Defined condition
I	2,088.8	10.08	250	Healthy
II	941.8	10.08	250	Damaged
III	0	10.08	250	Damaged

J. Eng. Mech. 2013.139:1185-1196.

To identify the stiffness and damping values of the 3-story symmetric structure in Stiffness Scenario I as a linear lumped-mass model [Fig. 4(a)], the nonlinear extended Kalman filter (Hoshiya and Saito 1984; Jeen-Shang and Yigong 1994) was preferred here to identify the parameters in the time domain. Assuming the mass is known, the state vector of the filter can be defined as $x = [z_1, z_2, z_3, \dot{z}_1, \dot{z}_2, \dot{z}_3, k_1, k_2, k_3, c_1, c_2, c_3]^T$, where z_i, $\dot{z}_i$, k_i, c_i are the displacement, velocity, stiffness parameters, and damping parameters of the ith story, respectively. The stiffness parameters were additionally adjusted based on the modal frequency analysis, and the analytical and experimental natural frequencies of the first three modes are listed in Table 2 for comparison. A close correlation between calculation and experiment was observed.

Table 2. Comparison between the Analytical and Experimental First Three Modal Frequencies of the 3-Story Aluminum Structure

Mode	Analytical frequency (Hz)	Experimental frequency (Hz)	Discrepancy (%)
1	1.827	1.831	−0.22
2	5.091	5.127	−0.70
3	7.262	7.227	−0.48

Fig. 5 shows the time history responses of the numerical simulation using the analytically identified model from Fig. 4(a) and those of the experimental structure in Scenario I (healthy), based on the N-S component of the 1995 Kobe earthquake. The agreement of the computed and measured time history responses is excellent.

The increased interstory stiffness to the first floor in reality was assessed based on the relationship between the measured force of the springs and the relative displacement on the first floor during the excitation using the least-square technique. The k_s denotes the attached spring stiffness value as the gradient of the linear force-displacement relationship, as shown in Fig. 6. The identified k_s were 2,088.8 and 941.8 N/m for Stiffness Scenarios I and II, respectively. The initial interstory stiffness of the first floor was assessed to be 7,702.5 N/m, including $k_s = 2{,}088.8$ N/m, so the corresponding stiffness reductions Δk_1 for different scenarios were 1,147 and 2,088.8 N/m, indicating α_1 being 14.9 (Scenario II) and 27.1% (Scenario III), respectively.

As discussed previously, the currently developed monitor algorithm takes the relative accelerations on each floor and the excitation as the inputs to the designed monitors. The integration time horizon t_h was assigned as 2 s beforehand. Fig. 7 illustrates the tracking

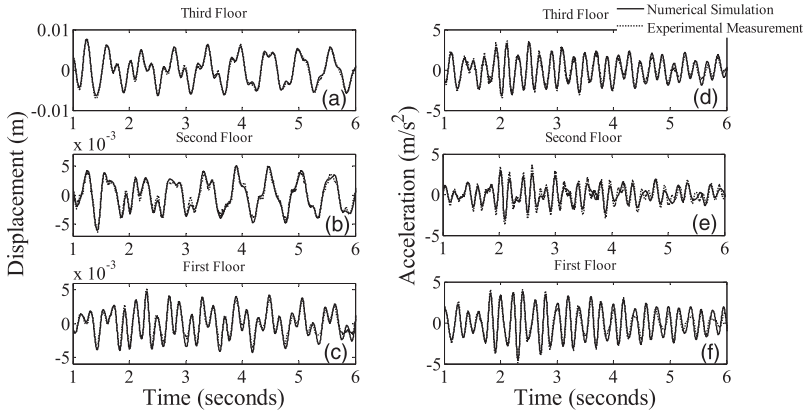

Fig. 5. Comparison of the dynamic responses between the numerical simulation and experimental measurement of the 3-story aluminum model in Stiffness Scenario I subjected to the N-S component of 1995 Kobe earthquake: displacements on the (a) third floor; (b) second floor; and (c) first floor and acceleration on the (d) third floor; (e) second floor; and (f) first floor

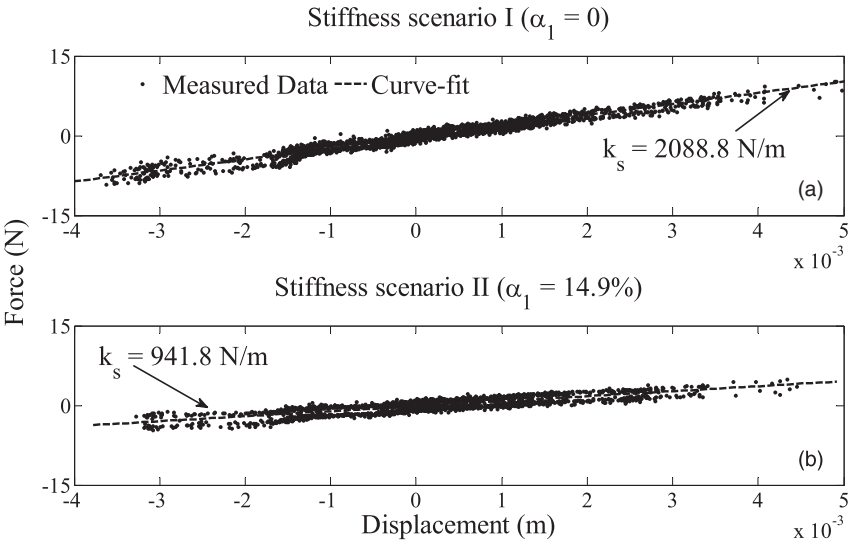

Fig. 6. Measured experimental data and the least-square fit displacement-force curves in (a) Stiffness Scenario I (healthy $\alpha_1 = 0$), and (b) Stiffness Scenario II (damaged $\alpha_1 = 14.9\%$)

J. Eng. Mech. 2013.139:1185-1196.

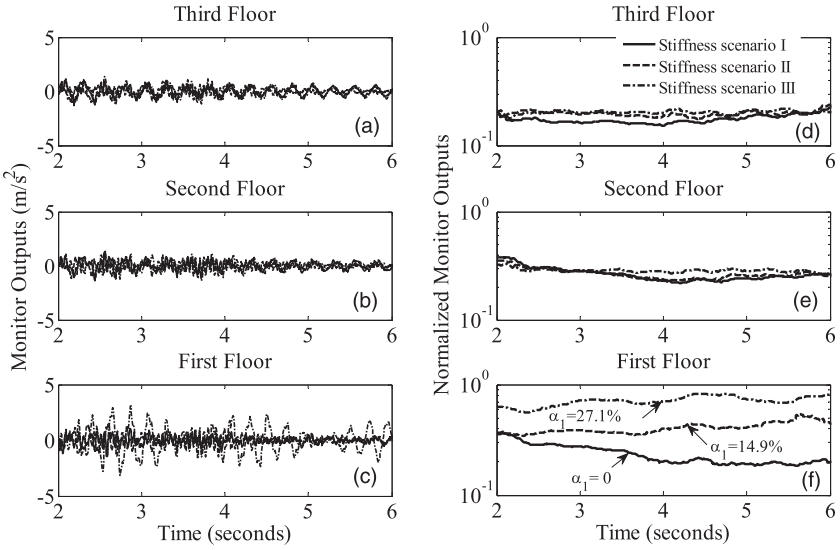

Fig. 7. Original and normalized monitor outputs for the 3-story experimental structure in different stiffness scenarios (monitor i for the ith floor): (a)–(c) are original monitor outputs and (d)–(f) are normalized monitor outputs for Scenarios I ($\alpha_1 = 0$), II ($\alpha_1 = 14.9\%$), and III ($\alpha_1 = 27.1\%$), respectively

results of different stiffness scenarios. Fig. 7(c) shows the monitor output on the first floor caused by the stiffness changes in different scenarios. In Fig. 7(f), the normalized monitor output shows that the damaged and the undamaged scenarios are readily distinguishable from each other. The normalized monitor outputs, as shown in Figs. 7(d and e), for the second and third floor remain stable and similar in different stiffness scenarios, indicating the similar stiffness condition on the second and third floor.

Comparison of Results between the Experimental Aluminum Model and Numerical Simulation Model

Because the monitor output is normalized with Eq. (18), the time interval of the simulation Δt may affect the numerical integration results. A convergence study of Δt on the normalized monitor output was performed, and the results are illustrated in Fig. 8 with different values of Δt ranging from 0.0005 to 0.08 s for numerical calculations on the mean values of the normalized monitor output $\bar{\ddot{r}}_{\text{norm},i}$. These are calculated from the relatively stable and flat part of the normalized monitor outputs $\ddot{r}_{\text{norm},i}$. In the experimental verification process, although response accelerations were measured experimentally with time, the normalized monitor output values ($\ddot{r}_{\text{norm}}$) were still calculated with $\Delta t = 0.004$ s and $t_h = 2$ s as defined in Eq. (18). The normalized monitor output of Stiffness Scenario III ($\alpha_1 = 27.1\%$) from both the experimental measurement and numerical simulation was selected. The mean values of the selected normalized monitor outputs were calculated and compared. It is seen that the mean value of the normalized monitor output converges when Δt becomes smaller than 0.018 s, both from the experimental model and the numerical simulation model. This convergence study may help justify the choice of $\Delta t = 0.004$ s in the current study as the converged value.

Fig. 9 compares the normalized monitor outputs $\ddot{r}_{\text{norm},1}$ of different stiffness scenarios for the first floor, generated by both the experimental structure and the current numerical simulation model. The experimental data are selected from Fig. 7(f). Three sets of numerical results were derived based on the numerical dynamic responses of the lumped-mass model from Fig. 4(a) with predetermined interstory stiffness changes. The SNR was assumed as 20 dB to simulate the noisy condition of the experiment. It was observed that the experimental and numerical normalized monitor outputs of the first floor were matching closely to each other in the

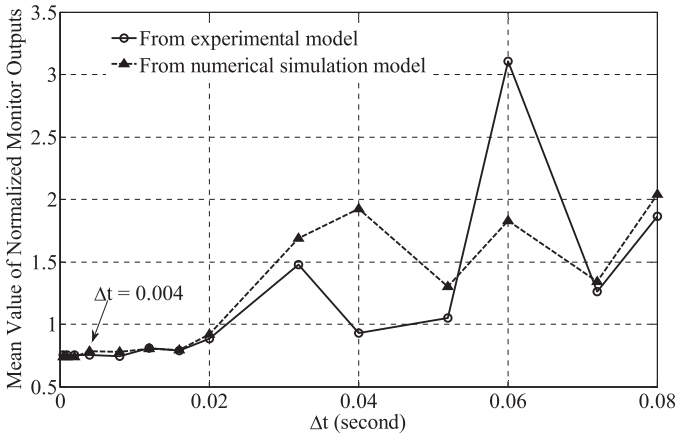

Fig. 8. Convergence study of the time interval of the numerical monitor calculation Δt for the mean value of normalized monitor output for the Damage Scenario III ($\alpha_1 = 27.1\%$) using different time intervals

three different stiffness scenarios. This experimental verification may add the validity that the stiffness changes can be estimated by the current interstory drift–based acceleration feedback method.

Damage Severity Estimation

To further ensure the confidence of the estimation of the damage in addition to the comparison as shown in Fig. 9, the difference in the mean values of the normalized monitor outputs $\bar{\ddot{r}}_{\text{norm},i}$ between the damaged and healthy cases was proposed as a damage severity indicator. The $\bar{\ddot{r}}_{\text{norm},i}$ is defined as $\Delta\bar{\ddot{r}}_{\text{norm},i} = \bar{\ddot{r}}_{\text{norm},i,\text{damaged}} - \bar{\ddot{r}}_{\text{norm},i,\text{healthy}}$. The relation between stiffness changes α_i and $\bar{\ddot{r}}_{\text{norm},i}$, may be plotted as a curve to predict or to interpolate stiffness changes as a means to estimate the damage severities. The numerical prediction curve of stiffness change may be obtained by computing the corresponding $\bar{\ddot{r}}_{\text{norm},i}$ from preset stiffness changes $\alpha_i = 0, 1, 5, 10, \ldots, 50, \ldots$. In the event of excitation, one can refer to the numerical prediction curve of stiffness change and simply linearly interpolate α_i. The procedure of developing the numerical prediction curve and evaluating the stiffness change is summarized in Fig. 10.

J. Eng. Mech. 2013.139:1185-1196.

The numerical prediction curve of the 3-story aluminum structure is plotted in Fig. 11. In Stiffness Scenario II with $\alpha_1 = 14.9\%$, the calculated $\bar{\ddot{r}}_{\text{norm},i}$ from the experimental measurement is 0.22, which is interpolated to predict the $\alpha_{1,\text{prediction}}$ as 13.9%, as shown in Fig. 11. Similarly in Scenario III, the $\bar{\ddot{r}}_{\text{norm},i}$ of 0.54 gives the prediction $\alpha_{1,\text{prediction}} = 25.8\%$. The discrepancies of the prediction stiffness changes in these two cases are 6.7 and 4.8%, respectively. This shows that the numerical prediction curve of stiffness change may be of practical value to estimate the stiffness changes in practice.

Twelve-Story Concrete Structure

The advantage of acceleration measurements over displacement measurement is one factor that has been considered. There are also some other practical issues that may need to be studied for damage prediction, such as the effect of different earthquakes with different characteristics, incomplete measurement, and different structural materials. To study these important factors, a 12-story RC concrete frame structure, as shown in Fig. 3(b), was selected to further evaluate the present method. There are three factors embedded in the choosing the present experiment study: (1) incomplete measurement; (2) different excitations with different characteristics; and (3) real damage occurrence and subsequent development in concrete structures.

As seen in Fig. 3(b), the dimensions of the plane section of the frame were 0.6 × 0.6 m, and the height of the frame was 3.6 m. The dead and live loads were simulated by lead-block units fixed on the plate of every floor, and the total mass of the simulated load was 19.4 kg for the typical floor and 19.7 kg for the roof floor. Seven accelerometers were placed on the ground level, second floor, fourth floor, sixth floor, eighth floor, 10th floor, and roof floor, collectively. The uni-/bi/tridirectional excitations were performed to the structure during the shaking table test. For simplicity of demonstration, only some of the cases with uni-directional excitations were chosen for experimental verification here, which were Cases 2, 3, 4, 8, 9, 10, and 17 in the original test setup. For convenience, the seven selected cases were renumbered in sequence as Cases 1–7, as listed in Table 3. The excitation data were taken from the N-S component of the 1940 El Centro earthquake, the N-S component of the 1995 Kobe earthquake, and the simulated Shanghai wave. The simulated Shanghai wave is not a naturally measured record and is provided in a building code for seismic design of buildings in Shanghai. Most of the experimental information and measured data are now available online (http://risedr.tongji.edu.cn/). Table 3 lists the setup and modal analysis results of the experimental structure in the selected cases. The first four-mode natural frequencies were estimated from the acceleration measurement on the roof floor.

Visual damage inspections were conducted during the test, and the observation is summarized in Table 4. It is commonly understood that the natural frequency may indicate the overall stiffness of the structure, and the decrease of the natural frequency implies the

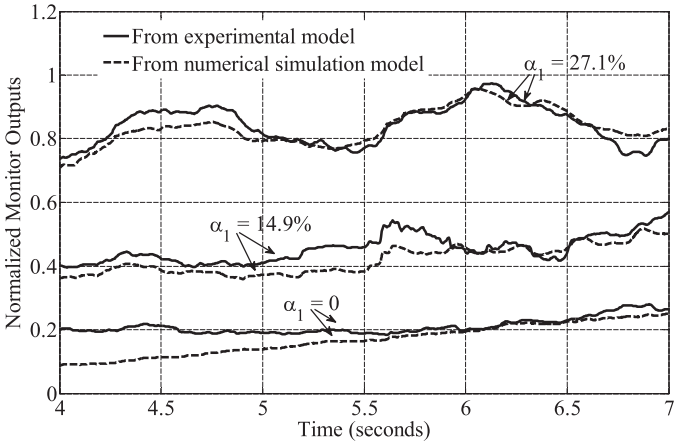

Fig. 9. Comparison of the normalized monitor outputs $\ddot{r}_{\text{norm},1}$ from the experimental model and numerical simulation model in Stiffness Scenarios I ($\alpha_1 = 0$), II ($\alpha_1 = 14.9\%$), and III ($\alpha_1 = 27.1\%$), with the time interval of the numerical monitor calculation Δt of 0.004 s and the SNR of the numerical simulation of 20 dB

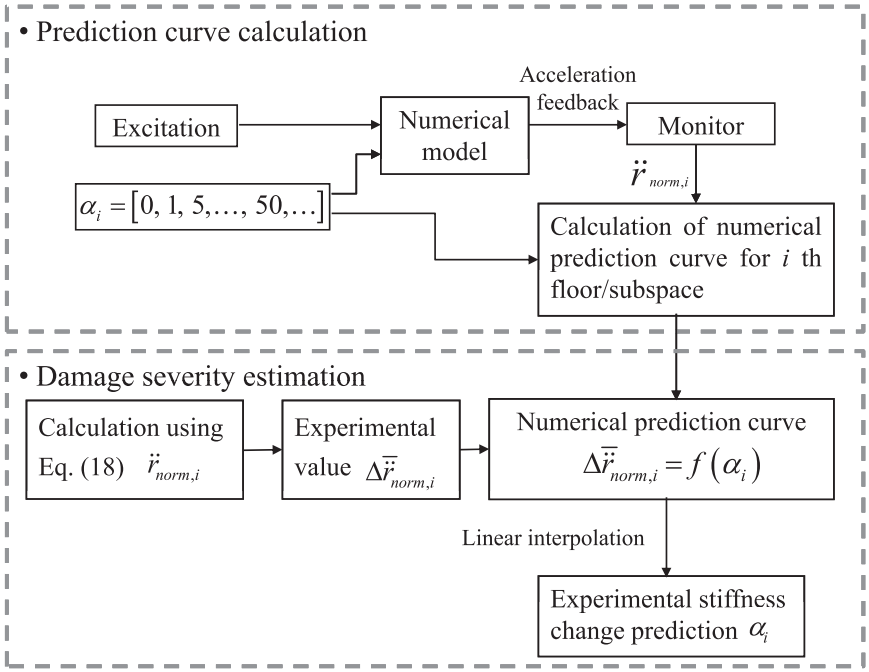

Fig. 10. Flowchart of prediction curve calculation and damage severity estimation

J. Eng. Mech. 2013.139:1185-1196.

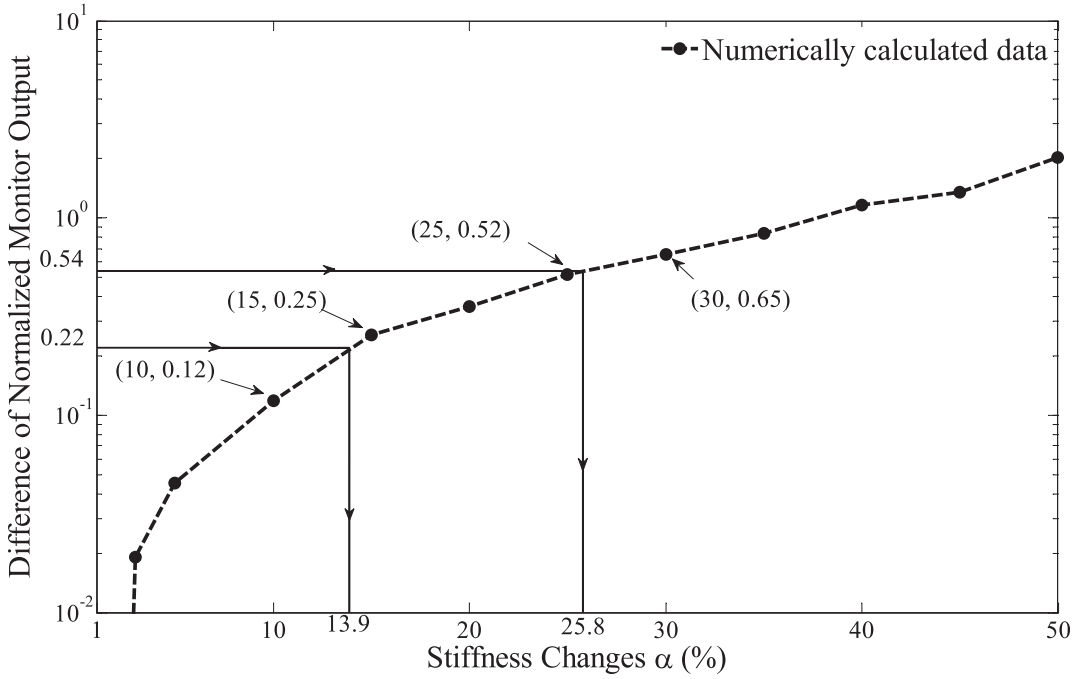

Fig. 11. Numerical prediction curve of the 3-story structure using a linear interpolation prediction approach to predict the stiffness values in two stiffness scenarios ($\alpha_1 = 14.9$ and 27.1%, respectively)

Table 3. Experimental Information and the Identified Modal Frequencies

Case number	External excitation	Peak acceleration (g)	Natural frequency (Hz)			
			1	2	3	4
1	El Centro	0.0921	3.74	14.45	27.65	40.11
2	Simulated Shanghai wave	0.0989	3.49	14.45	27.65	40.36
3	Kobe	0.0919	3.49	14.70	27.15	40.61
4	El Centro	0.2598	3.49	13.70	26.66	40.11
5	Simulated Shanghai wave	0.2660	2.49	13.70	26.91	40.11
6	Kobe	0.2812	2.24	10.71	21.18	32.64
7	El Centro	0.3985	2.24	9.97	19.43	30.64

Note: The sampling frequency is 255 Hz.

stiffness degradation of the structure. It is noted from Table 3 that the first four modal frequencies decreased noticeably in the chosen cases. This agrees with the damage inspection results in Table 4. The fundamental frequency decreased from 3.49 to 2.49 Hz after Case 5, which agrees with the first visible crack occurrence in the same case. The crack development after Case 7 was also observed by the decreases of all the identified four modal frequencies. The comparison of the fundamental frequency change and the damage inspection outcome is illustrated in Fig. 12, and the typical frame damage is also shown in Fig. 12. This experimental study was focused on the comparisons among the results on structural health condition tracking of the present algorithm, the changes in modal frequency, and the outcome of visual damage inspection during the current study on the damage occurrence, development, and location. The damage severity is not discussed in this section because of the lack of the accurate estimation of the stiffness reduction caused by the concrete cracks.

The experimental structure was first simplified and condensed into a 36 beam-column element numerical model. Each element has three degrees of freedom at each end, which are longitudinal displacement, transverse deflection, and an angle of rotation. The numerical model was then reduced into a six-degrees-of-freedom lumped-mass model for health monitoring using the model simplifying technique (Wrobleski and Yang 2003; Lin and Yang 2009). This simplification presents six monitoring subspaces for the 12-story experimental structure as shown in Fig. 13. The division of the monitoring areas depends on the accelerometer placement, and every subspace corresponds to a designed health monitor. In this experimental study, every two neighboring floors from the first floor to the roof floor composed a separated monitoring area; for example, the third and fourth floor as the second monitoring subspace under Monitor 2, which is also shown in Fig. 13. Table 5 reports the first five-mode natural frequencies of the two numerical models and

Table 4. Summary of the Damage Observation during the Selected Cases

Cases	Description of damage observation
1–4	No crack was observed on the frame components
5 and 6	Vertical crack occurred on the frame beams of the fourth floor after Case 5, and the width of crack was smaller than 0.05 mm
7	Vertical cracks on the frame beams of the third to sixth floor developed; the width of the cracks was $\sim 0.08 - 0.15$ mm

J. Eng. Mech. 2013.139:1185-1196.

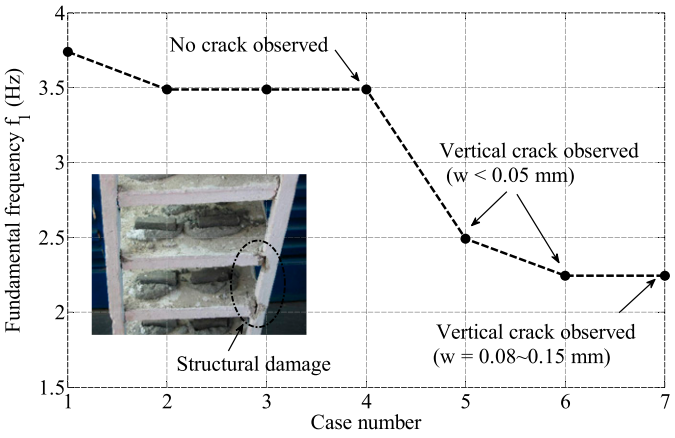

Fig. 12. Fundamental frequency changes, the three observations during the selected cases, and the typical frame beam cracks after the shaking table test in the subgraph, where w denotes the width of the cracks

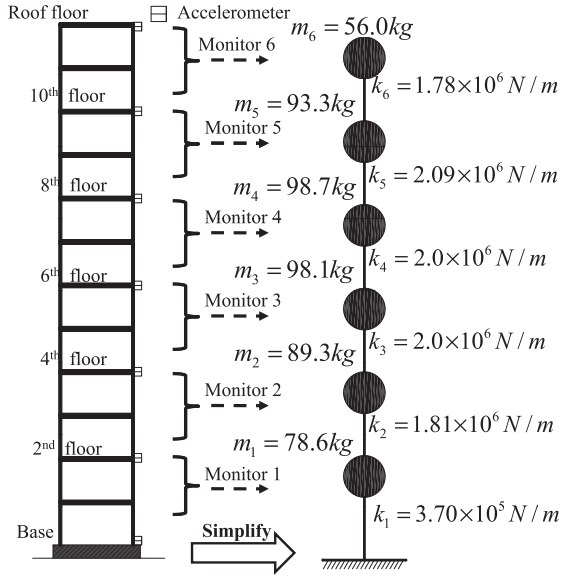

Fig. 13. Experimental accelerometer placement, the simplification from the beam-column element numerical model to the lumped-mass model using the model simplifying technique (Wrobleski and Yang 2003; Lin and Yang 2009), and the designed health monitors distribution

the experimental structure. The simplified lumped-mass model, with the mass and stiffness parameters illustrated in Fig. 13, agrees with the experimental structure on the modal frequencies listed in Table 5. The simplified lumped-mass model was then used in the study to track the health condition of the structure. Here only the normalized monitor outputs in different cases are shown in Figs. 14 and 15 for structural health condition tracking, which are compared with the modal frequency analysis results (Table 3; Fig. 12) and damage observation during the shaking table test (Table 4).

Figs. 14(b and c) show that the early-stage structural damage occurred in the second monitored subspace and slightly in the third subspace. This agrees with the indication of the 6.7% fundamental frequency decrease from 3.74 to 3.49 Hz. Although the damage was not substantial enough to be identified by visual inspection as described in Table 4, it is nonetheless partially proved from the first

Table 5. Comparison between the Analytical and Experimental Natural Frequencies of the 12-Story Concrete Structure (Case 1)

Mode	Experimental frequency (Hz)	Analytical frequency of the 36 beam-column element numerical model (Hz)	Analytical frequency of the simplified six-degrees-of-freedom lumped-mass model (Hz)
1	3.74	3.79	3.73
2	14.45	13.49	14.65
3	27.65	25.79	25.30
4	40.11	39.40	34.25
5	58.79	51.17	41.18

visible crack occurrence on the fourth floor, indicating the early damage development in this area. This implies that the damage location information is available even in its early developing stage with the proposed method. From Cases 2–4, the normalized outputs of Monitors 4, 5, and 6, as illustrated in Figs. 14(d, e, and f), respectively, nearly remained stable in different cases, indicating no significant damage occurrence and development on the seventh floor to the roof floor. Because the excitation inputs and the amplitude of the earthquake inputs were different during these cases, Fig. 14 may indicate (1) the effectiveness of decomposition of damage coupling effect in the proposed algorithm; (2) the stability of the normalization method in Eq. (18) when the peak acceleration has increased from 0.0921 (Case 1) to $0.2598g$ (Case 4); and (3) independence of different earthquakes from Cases 1–3.

It is noted in Table 4 that most of the observed damage occurrence and development were on the fourth floor. The normalized monitor outputs of Monitor 2 in Cases 1, 6, and 7 are illustrated in Fig. 15 to correlate the frequency decrease and the visual inspection result. The solid lines are distinguishable among each other, which correlate to the significant fundamental frequency decrease from 3.49 to 2.24 Hz between Cases 1 and 6, and the crack width development from $<$0.05 to 0.08–0.15 mm between Cases 6 and 7. The numerical simulation based on the simplified lumped mass model was performed to estimate the stiffness reduction of the second subspace in Cases 6 and 7. The normalized outputs of Monitor 2 are shown in dashed lines with the preset stiffness reduction factor α_2 as 50 and 65% in Cases 6 and 7, respectively. In the numerical simulation, Δt was 0.0039 s, the SNR was 30 dB, and the integration time horizon t_h was 4 s. It is seen in Fig. 15 that the normalized monitor output curves both from the experimental measurement and numerical simulation agree fairly with each other in the three selected cases. Additionally, the first three modal frequencies of the numerical models in Cases 6 and 7 with the updated stiffness losses of the six subspaces are provided in Fig. 15, showing the improved agreement with the experimental frequencies in Table 3.

Noise Effect

The illustrative 3-story shear beam model and the N-S component of the ground acceleration of the 1940 El Centro earthquake, previously used in the numerical simulation section, are selected here to further study the effects of the measurement noise on the damage detection. Different stiffness changes on the first floor, ranging from 1 to 40%, are assumed. For the sake of simplicity, the Gaussian white noise is assumed and added into the measurements. The variations of the mean value of the normalized monitor output with α under different measurement noise levels are shown in Fig. 16. The normalized monitor output increases as α increases, and such an increase is more apparent for lower noise level. The mean value of the normalized monitor outputs shows a relatively slight increase for

J. Eng. Mech. 2013.139:1185-1196.

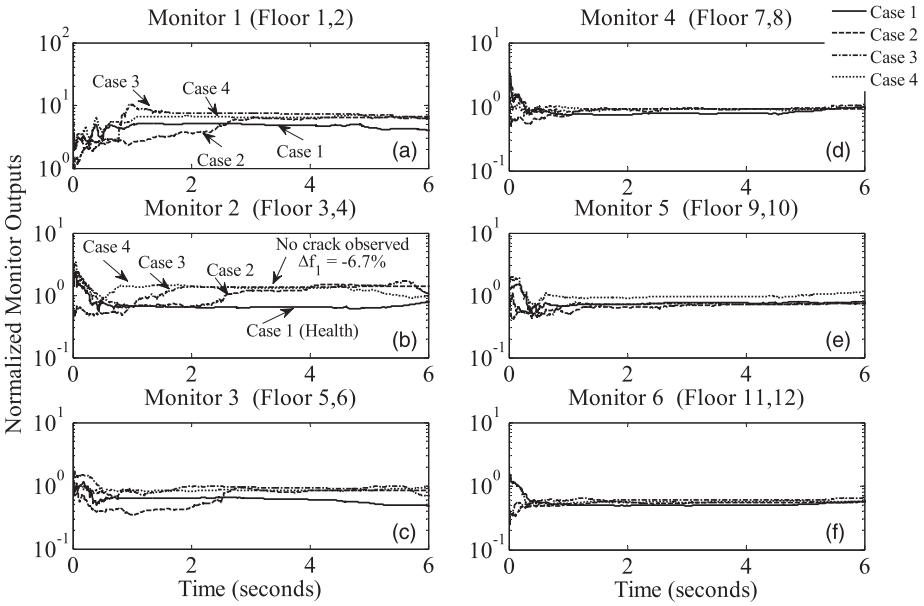

Fig. 14. Normalized monitor outputs in different excitation cases (Cases 1, 2, 3, and 4 as defined in Table 3) with six monitors on six lumped masses, respectively, with each representing two consecutive floors

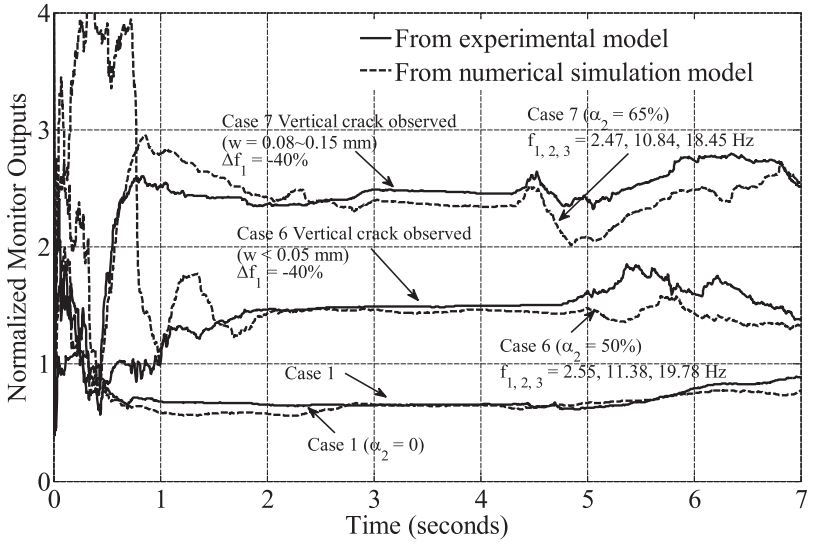

Fig. 15. Normalized monitor outputs of Monitor 2 for the third and fourth floor in different excitation cases (Cases 1, 6, and 7), where *w* denotes the width of the cracks

SNRs <40 dB when there is small stiffness change ($\alpha_1 < 10\%$). This observation indicates that the small damage may not be detectable in these noise-polluted cases. However, the noise effects are not significant compared with the noise-free case for relatively large stiffness changes ($\alpha_1 > 15\%$) when the SNRs are larger than 30 dB in this particular case.

Concluding Remarks

An interstory drift–based acceleration feedback method for structural health monitoring was presented in this study. It is demonstrated numerically and experimentally with examples that the currently developed interstory drift–based acceleration feedback algorithm performs well on the tracking of stiffness change. The tracking performance of the present proposed method, in terms of small and sudden stiffness changes, seems to be more pronounced over the previous displacement method (Ma et al. 2005) and similar to the previous acceleration method (Sebastijanovic et al. 2010) during the comparison through current illustrative numerical examples.

The interstory drift–based acceleration feedback method was systematically validated using a 3-story aluminum frame structure and a 12-story concrete frame structure, with damage simulated by spring attachments and actual concrete cracks, respectively. The results of the 3-story model show that the assumed 14.9 and 27.1% interstory stiffness change on the first floor was successfully identified and predicted with favorable agreement through a proposed numerical prediction curve of stiffness change. The time interval of the simulation Δt should be selected carefully when calculating the normalized monitor outputs. The occurrence, development, and location of the

J. Eng. Mech. 2013.139:1185-1196.

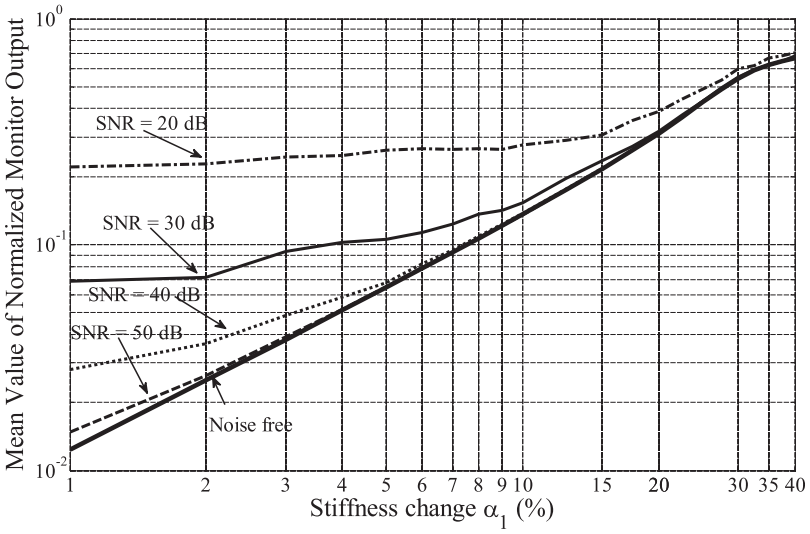

Fig. 16. Noise effect on mean value of normalized monitor outputs of the 3-story model

crack in the 12-story model were determined by the interstory drift–based acceleration feedback method. The incomplete measurements, the different earthquake inputs, the different input energy levels, the real structural cracks in concrete, and the increase in the number of stories may not affect the structural health tracking performance of the present method. Particularly, before the observed crack occurrence on the fourth floor of the concrete structure, the damage location was indicated quite clearly by Monitor 2 when the first four modal frequencies already indicated the stiffness degradation of the structure.

Although the earthquake excitations are selected as illustrative inputs in this study, the reproducible excitations such as shakers can also be used for the proposed method with similar derived equations. The stiffness changes can then be tracked through comparison of responses of healthy structure and damaged structure.

To continue the present global vibration health monitoring method study, a logical next step appears to be the integration of the local nondestructive evaluation and the structural control, i.e., incorporation of the control into the present methods.

Acknowledgments

This study is sponsored by National Science Foundation Grant No. CMS 1014958, and the support of program director, Bruce M. Kramer, is gratefully acknowledged. Financial support from the China Scholarship Council for J. Shan's work at the University of California, Santa Barbara, as a visiting scholar is highly appreciated.

References

Celebi, M., Sanli, A., Sinclair, M., Gallant, S., and Radulescu, D. (2004). "Real-time seismic monitoring needs of a building owner—And the solution: A cooperative effort." *Earthq. Spectra*, 20(2), 333–346.

Curadelli, R. O., Riera, J. D., Ambrosini, D., and Amani, M. G. (2008). "Damage detection by means of structural damping identification." *Eng. Struct.*, 30(12), 3497–3504.

Doebling, S. W., Farrar, C. R., Prime, M. B., and Shevitz, D. W. (1996). *Damage identification and health monitoring of structural and mechanical systems from changes in their vibration characteristics: A literature review*, Los Alamos National Laboratory, Los Alamos, NM.

Gao, Y., Spencer, B., Jr., and Bernal, D. (2007). "Experimental verification of the flexibility-based damage locating vector method." *J. Eng. Mech.*, 133(10), 1043–1049.

Ghanem, R., and Ferro, G. (2006). "Health monitoring for strongly nonlinear systems using the ensemble Kalman filter." *Struct. Contr. Health Monit.*, 13(1), 245–259.

Hoshiya, M., and Saito, E. (1984). "Structural identification by extended Kalman filter." *J. Eng. Mech.*, 110(12), 1757–1770.

Jeen-Shang, L., and Yigong, Z. (1994). "Nonlinear structural identification using extended Kalman filter." *Comp. Struct.*, 52(4), 757–764.

Lin, C. H., and Yang, H. T. Y. (2009). "Structural health monitoring for frame structure with semi-rigid joints." *Proc., SPIE Smart Structures/NDE*, Vol. 7292, SPIE, Bellingham, WA.

Liu, P. L. (1995). "Identification and damage detection of trusses using modal data." *J. Struct. Eng.*, 121(4), 599–608.

Ma, T. W., Yang, H. T., and Chang, C. C. (2005). "Structural damage diagnosis and assessment under seismic excitations." *J. Eng. Mech.*, 131(10), 1036–1045.

Pandey, A. K., Biswas, M., and Samman, M. M. (1991). "Damage detection from changes in curvature mode shapes." *J. Sound Vibrat.*, 145(2), 321–332.

Porter, K., Mitrani Reiser, J., and Beck, J. L. (2006). "Near real time loss estimation for instrumented buildings." *Struct. Des. Tall Spec. Build.*, 15(1), 3–20.

Salawu, O. S. (1997). "Detection of structural damage through changes in frequency: A review." *Eng. Struct.*, 19(9), 718–723.

Sebastijanovic, N., Yang, H. T. Y., and Ma, T. W. (2010). "Detection of changes in global structural stiffness coefficients using acceleration feedback." *J. Eng. Mech.*, 136(9), 1187–1191.

Skolnik, D. A., and Wallace, J. W. (2010). "Critical assessment of interstory drift measurements." *J. Struct. Eng.*, 136(12), 1574–1584.

Vanik, M., Beck, J., and Au, S. (2000). "Bayesian probabilistic approach to structural health monitoring." *J. Eng. Mech.*, 126(7), 738–745.

Wrobleski, M. S., and Yang, H. T. Y. (2003). "Identification of simplified models using adaptive control techniques." *J. Struct. Eng.*, 129(7), 989–997.

Yang, J., Wu, J., and Agrawal, A. (1995). "Sliding mode control for seismically excited linear structures." *J. Eng. Mech.*, 121(12), 1386–1390.

Yang, J. N., Lin, S., Huang, H., and Zhou, L. (2006). "An adaptive extended Kalman filter for structural damage identification." *Struct. Contr. Health Monit.*, 13(4), 849–867.

Yang, J. N., Pan, S., and Lin, S. (2007). "Least-squares estimation with unknown excitations for damage identification of structures." *J. Eng. Mech.*, 133(1), 12–21.